Micron 42 (2011) 366–375

Contents lists available at ScienceDirect

Micron

journal homepage: www.elsevier.com/locate/micron

A microscope configuration for nanometer 3-D movement monitoring accuracy

Yevgeny Beiderman[a], Avigail D. Amsel[b], Yaniv Tzadka[b], Dror Fixler[b], Vicente Mico[c], Javier Garcia[c], Mina Teicher[a], Zeev Zalevsky[b,*]

[a] Department of Mathematics, Bar Ilan University, Ramat Gan 52900, Israel
[b] School of Engineering, Bar Ilan University, Ramat Gan 52900, Israel
[c] Departamento de Óptica, Universitat de València, c/Dr. Moliner, 50, 46100 Burjassot, Spain

ARTICLE INFO

Article history:
Received 31 December 2009
Received in revised form 8 April 2010
Accepted 31 May 2010

Keywords:
Fourier optics
Speckle
Backscattering
Movement monitoring

ABSTRACT

In this paper we present a new microscopy configuration based upon temporal tracking of a secondary reflected speckle by imaging the speckle through properly defocused optics. The configuration is used to monitor three-dimensional (3-D) spontaneous contraction of rat cardiac muscle cells while achieving nanometer tracking accuracy at a rate of 30 frames per second (fps) without using interferometric recording. Estimation of the change in the optical path of accuracy of 50 nm in the transverse direction and of 200 nm in the axial direction was achieved.

1. Introduction

Movement tracking of cells in microscopy has important applications in biological studies. For instance, the ability of a heart to pump blood depends on the interaction between its components. This includes a broad variety of cell types such as muscle cells and connective tissue (Burlew and Weber, 2000). Specific cell types of interest in the heart are myocytes which exhibit spontaneous movement even as isolated cells. As the cells come closer together they develop a synchronized contraction and thus they provide an excellent model for in vitro studies. The ability to trace various physiological events during contraction cycles of single cardiomyocytes has greatly increased in recent years (Fixler et al., 2003), and such measurements have the potential to contribute to the fundamental understanding of cellular stimulation and activation. For instance, during contraction cycles of myocardial tissue, rapid changes within single cells can be measured and correlated, e.g., membrane potential, cytosolic Ca^{2+} concentration, and intracellular pH, compared to shortening and tension generation (Calaghan and White, 1999; Spurgeon et al., 1990).

Movement tracking in microscopy can be obtained using various interferometeric and holographic approaches applied mainly in transmission (Ikeda et al., 2005; Marquet et al., 2005). The most common approach is to use digital interferometry in either an on or off axis phase shift configuration (Yamaguchi and Zhang, 1997; Schnars and Jüptner, 1994). Improvement and adjustment of those approaches for real time measurement were presented in Shaked et al. (2009a,b,c). However, all those approaches are working in transmission and thus they allow detection of only transverse movement. Neither axial movement nor tilts that do not involve a change in the refraction index of the cells can be detected using those approaches since such movements do not affect the interference state of the resulting image.

Recently, a new microscopy configuration allowing high accuracy non-contact detection of axial and tilted movement was developed (Zalevsky and Garcia, 2008; Zalevsky et al., 2009). This approach, which was demonstrated experimentally for the detection of voice signals and subjects' heart beats from ranges of tens of meters, is based upon temporal tracking of the reflected secondary speckle pattern while defocusing the imaging lens of the camera.

Note that we distinguish between two types of speckle: primary and secondary. Primary speckle pattern is obtained when a surface is illuminated by a laser beam passing through a diffusive mask such as a ground glass. Primary speckle pattern is created due to projection and it is obtained even in case that the illuminated object has no roughness. Secondary speckle pattern is obtained on a detector plane by directly illuminating (with a laser) an object with rough surface. This pattern is created due to roughness of the illuminated surface.

Usage of speckle for movement tracking was already demonstrated before (Leedertz, 1970) however no defocusing was applied there. The defocusing of the lens allows translation of the tilt movement into lateral movement of the random speckle pattern (tracking this lateral movement is a simple numerical task that can

* Corresponding author.
E-mail address: zalevsz@eng.biu.ac.il (Z. Zalevsky).

0968-4328/$ – see front matter © 2010 Elsevier Ltd. All rights reserved.
doi:10.1016/j.micron.2010.05.020

be fulfilled using basic correlation based algorithm), rather than the variation of this random pattern as obtained without performing the defocusing.

In this paper we show how capturing a video sequence is used for tracking the 2-D movement of the speckle patterns and obtaining detection of tilting (if present) and transverse movement. We perform correlation between each two temporally adjacent frames of the video sequence (full frame correlation) for detecting of not only the position, but also the value of the correlation peak between the two sequential frames. The value of the correlation peak designates the relative change in the randomness of the speckle pattern (and not the shift of the pattern). This change in the pattern itself corresponds to the axial movement. Thus, in this paper we track the transverse and the tilting movement of the cells by observing the shifts of the correlation peaks. We also observe the axial movement by comparing the value of the correlation peak to a calibration reference look up table.

The novelties presented in this paper include the development of 3-D movement monitoring module providing nanometer accuracy and which can be applied for transmissive microscope configuration. In addition it is the first time, to the best of our knowledge, that a 3-D movement tracking of *several spatial segments* within cardiac muscle cells was performed.

It is important to stress here that the implemented technique is far from being identical to speckle pattern vibrometry approaches developed in the 70 s. Speckle pattern vibrometry cannot detect titling nor full 3-D movement. It was applied to rigid reflective objects and not transparent cells and usually uses Doppler shifts to perform its structural measurement (a completely different technique and configuration). In addition to the configuration itself which is different, the application itself involving contractual movement of cardiac myocyte cells in 3-D with a precision of tens of nanometers, is novel. Moreover, speckle pattern vibrometry suffers from speckle "dropouts", due to the changing of the speckle pattern while the object moves. This reduces the accuracy of the movement mapping process. Contrarily, in our case, the pattern is constant, while the movement of the object causes the pattern to be shifted rather than to change.

Section 2 presents the theoretical explanation and the modeling, while the experimental setup is given in section 3. The experimental results for the 3-D tracking of the entire cell are presented in Section 4. In Section 5 we experimentally extract the 3-D map and flow distribution of spatial segments *inside* cardiac muscle cells. The paper is concluded in Section 6.

2. Theoretical explanation and modeling

Secondary speckle pattern can simply be described as a self-generated random assembly of spots of light. An example of the speckle pattern as used in our system under proper defocusing is shown in Fig. 1. By the term of proper defocusing we refer to defocusing the imaging lens by moving it towards the far field such that the speckle in the pattern becomes fully recognizable (speckle spot size is increased, becoming more than a single pixel in the detector). While the spatial size of the speckle on the detector plane is proportional to the product between the wavelength and the f-number, moving the lens out of focus towards the far field causes the f-number ($F_{\#}$) to become larger and therefore makes the pattern more recognizable. Thus, the defocusing is made until high contrast and recognizable (in its resolution) speckle pattern is formed.

As stated before, the proper defocusing causes the tilting movement of the cells to be translated into lateral movement of the speckle as observed by our imaging system. We use correlation as a tool for the extraction of the relative movement of the speckle pattern of temporally sequential images in the captured video. The relative shift of the correlation peak from the origin is linearly proportional to the actual tilting movement of the cells. Finally, all relative movements are cumulatively summarized in the total movement vector. The same procedure is done for the values of the correlation peaks that designate axial (Z-axis) movement. Fig. 2 presents the flow chart of the algorithm. Thus, 3-D movement estimation includes computation of the correlation peak for the captured speckle patterns while from the position of the peak we extract the information regarding the transverse movement and the tilting of the object (Zalevsky and Garcia, 2008; Zalevsky et al., 2009), and from its value we obtain the information regarding the axial movement.

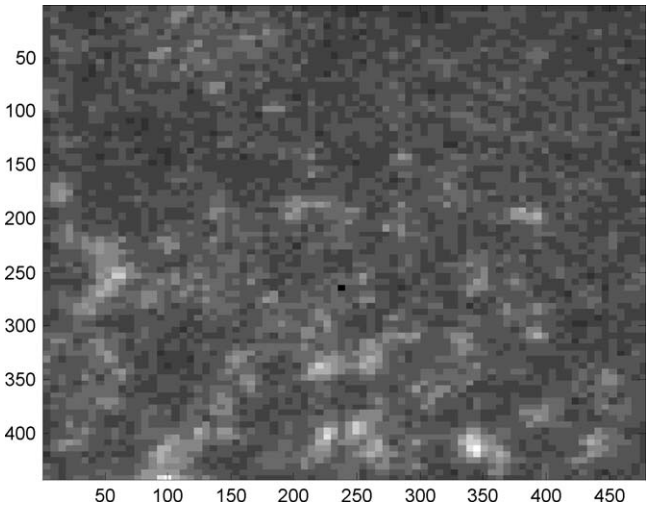

Fig. 1. Speckle pattern as obtained by the properly defocused camera of the microscope.

The dependence of the value of the correlation function on the transverse and the axial positions may be modeled as follows: with the assumption of circular uniform-intensity at the object plane (being the diffusive source that generates the secondary speckle) the correlation function of the intensity between two points separated in the transverse plane by a radial distance s and which are located at distance z from the diffusive object may be estimated as (Leushacke and Kirchner, 1990):

$$\Gamma_{\text{Transversal}}(s) = \bar{I}^2 \left(1 + 2\left|\frac{J_1\left(\pi\Phi s/\lambda z\right)}{\pi\Phi s/\lambda z}\right|\right) \tag{1}$$

where $\bar{I}$ is the mean of the intensity in the output plane, Φ is the diameter of the illumination beam, J_1 is the first kind Bessel function, λ is the optical wavelength and z is the axial distance.

With respect to the axial extent of the speckle, the problem reduces to the calculation of the axial correlation function of the intensity between two points separated axially by Δz. In this case, with the same assumptions as in the transverse case plus the requirement that Δz will be small compared with z, the correlation of intensity results with (Leushacke and Kirchner, 1990):

$$\Gamma_{\text{Longitudinal}}(\Delta z) = \bar{I}^2 \left(1 + 2\left|\sin c\left(\Delta z \cdot \frac{\Phi^2}{8\lambda z^2}\right)\right|\right) \tag{2}$$

3. Experimental setup

The work presented in this paper combines the depicted configuration suited to an inverted microscope with an oblique illumination of the inspected cells with green laser at wavelength of 532 nm. The setup is very simple and includes only a

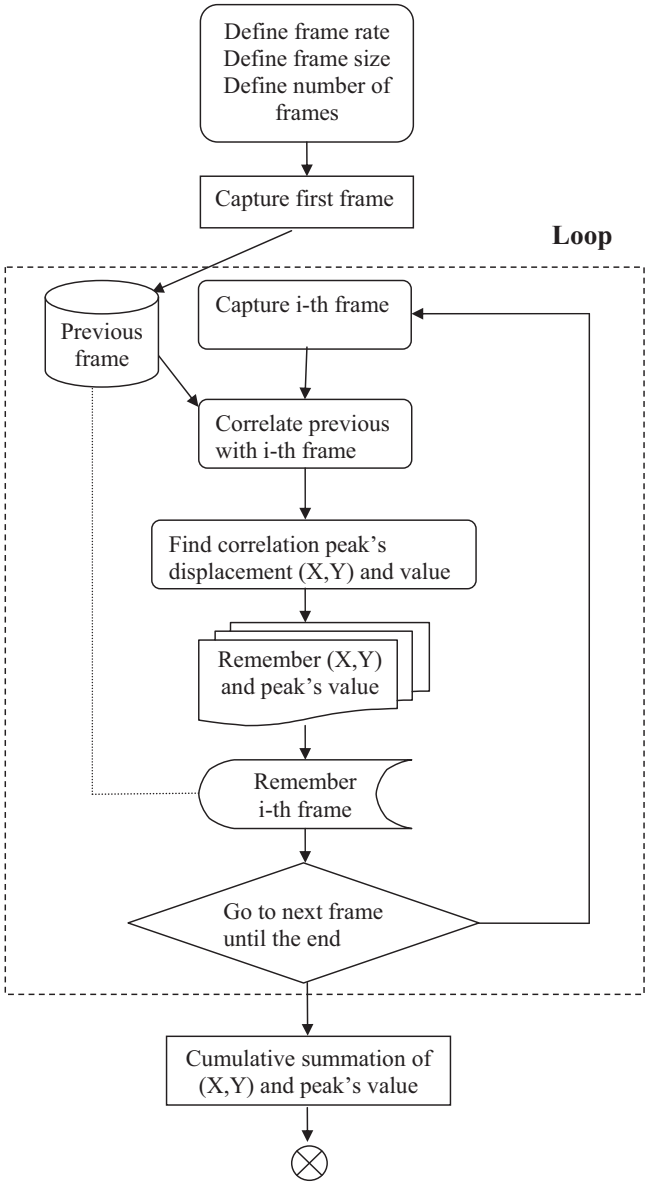

Fig. 2. Flow chart of the algorithm.

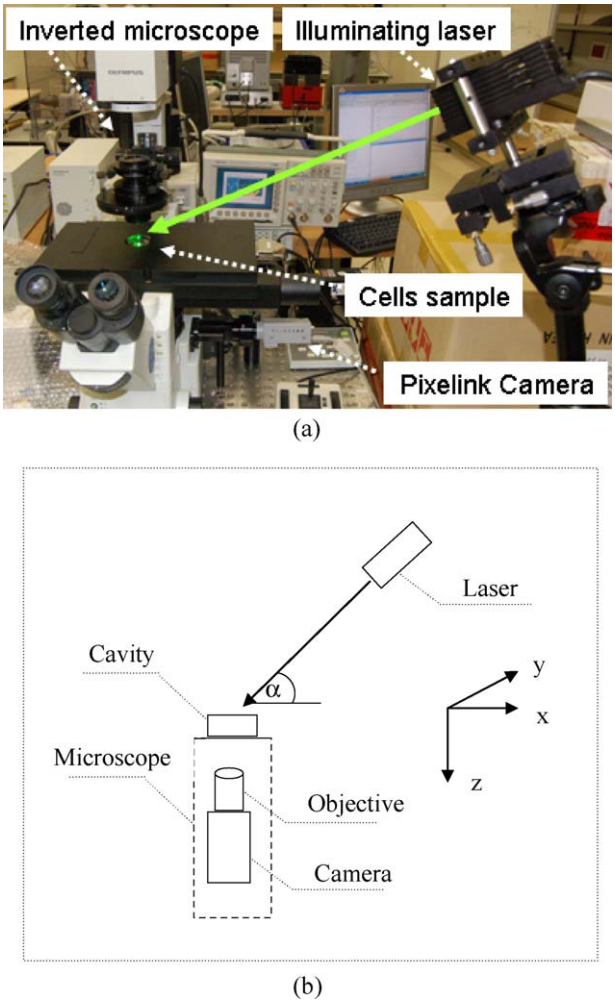

Fig. 3. (a) Image of the experimental setup. (b) Schematic sketch of the experimental setup.

green laser to illuminate the inspected object (in order to generate the secondary reflected speckle) and a camera connected to the microscope optics (being slightly defocused) that captures the random speckle patterns. The image of the experimental setup is given in Fig. 3(a) and its schematics in Fig. 3(b). The relevant coordinate system is described in Fig. 3(b) where the *X*–*Y* relates to a transverse plane and *Z* is axial axis. Further, the camera captures a video sequence, while Matlab software tracks the movement of the reflected/scattered speckle patterns and extracts the 2-D projection of the 3-D movement of the cells (including tilting movement if exists). In addition the system can track the axial movement of the objects by observing the value (and not the position) of the correlation between sequential speckle images.

This configuration has two significant advantages over existing approaches. First, the experimental setup is not an interferometric one and thus it needs no reference arm. This is a very important difference in comparison with previous work since it significantly simplifies the experimental setup while retaining the nanometer accuracy of holographic and digital phase approaches (Dubois et al., 2006; Park et al., 2007). Please note that in our approach we measure in high accuracy the movement of the cells and not their position.

Second, although the discussed method is demonstrated in transmissive configuration, we illuminate obliquely the sample at an angle (denoted by α at Fig. 3(b)) which is higher than the one defined by the NA of the lens. That is, the DC term of the illumination (non-scattered illumination beam) is not transmitted through the microscope lens and only scattered components are. This is similar to a reflective configuration where the image comes without a background. Such an illumination configuration (high oblique angle illumination in transmission or reflection configurations) maintains detection of cells transverse movement with the same accuracy as in transmission interferometry and additionally allows nanometer accuracy detection of axial movement and tilts of the cells which cannot be detected at all in transmission interferometry.

Cell culture and sample preparation for measurements were as follows: Rat cardiac myocytes were isolated as previously described in Fixler et al. (2002). Briefly, hearts from newborn rats were rinsed in phosphate buffered saline (PBS), cut into small pieces and incubated with a solution of proteolytic enzymes-RDB (Biological Institute, Ness-Ziona, Israel), prepared from a fig tree extract. The RDB was diluted 1:100 in Ca^{2+} and Mg^{2+}-free PBS at 25 °C and incubated with the heart fragments for several cycles of 10 min each. Separated cells were then suspended in Dulbecco's Modified Eagle's

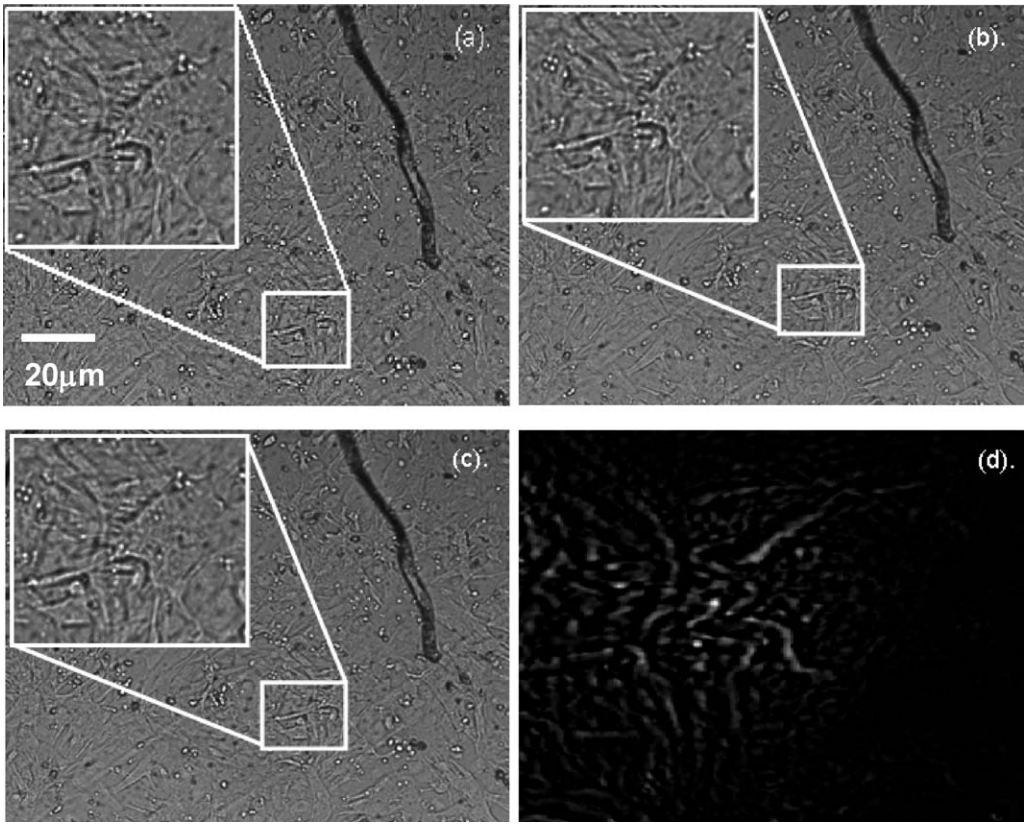

Fig. 4. Images sequence extracted from video using regular white light illumination (not laser). (a) Before contraction. (b) Maximum contraction. (c) Maximum expansion after contraction. (d) Image of differences for the zoomed region appearing in the white rectangle in (a) and (b). Horizontal bar in (a) corresponds to size of 20 μm.

Medium (DMEM) containing 10% inactivated horse serum (Biological Industries, Kibbutz Beit Haemek, Israel) and 2% chick embryo extract, and centrifuged at 300 × *g* for 5 min.

The suspension of the cells was diluted to 1×10^6 cells/ml, and 1.5 ml was placed in 35-mm plastic culture dishes on collagen/gelatin-coated cover glasses. The cultures were incubated in a humidified atmosphere of 5% CO_2, 95% air at 37 °C. Confluent mono-layers exhibiting spontaneous contractions were developed in culture within 2 days. The growth medium was replaced after 24 h and then every 3 days. As reference part of the cultures on day 4 were treated with 0.5–5 μM of doxorubicin (Biological Industries, Kibbutz Beit Haemek, Israel) for 18 h and then with drug-free growth medium for an additional 24 h.)

Cell samples were grown on microscope cover slips and placed under a microscope where they exhibited spontaneous contractions. The microscope we used was an Olympus inverted epifluorescence Olympus IX81 microscope equipped with an external green laser module. The illuminated field

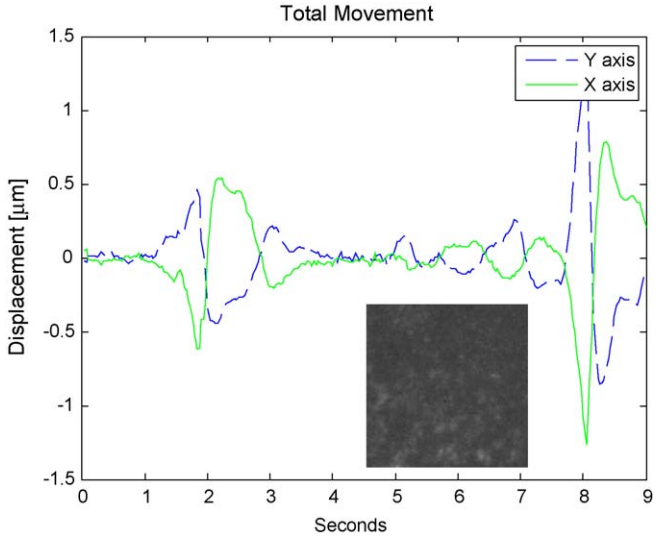

Fig. 5. *X* and *Y* axes movement in two different video sequences that were obtained using a 10× objective, region of interest of 80 × 80 pixels and rate of 30 fps. In the lower part of the image one may see the diffused speckle pattern used to perform the movement tracking.

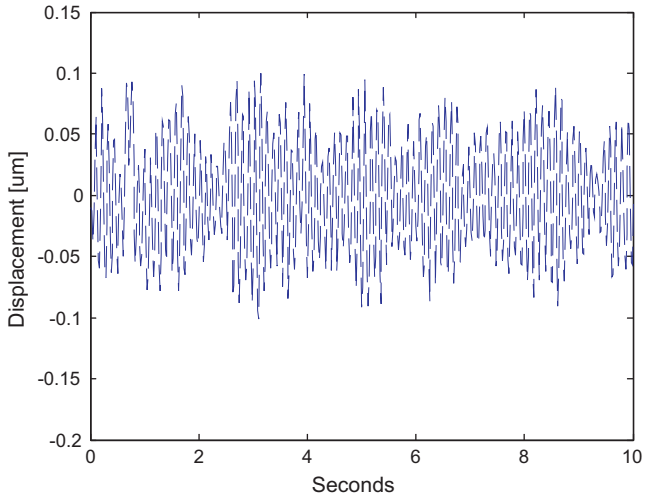

Fig. 6. *X* axis transverse movement of a reference cells (dead cells) obtained after analyzing the video sequence.

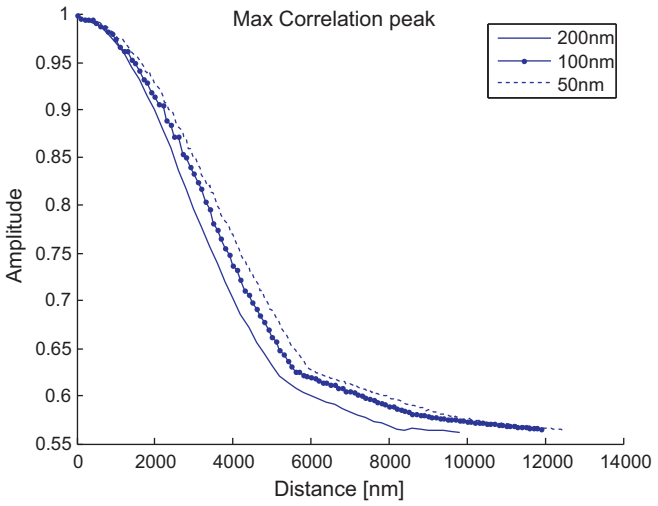

Fig. 7. Experimental measurement of the axial movement that is obtained by mapping the amplitude of the correlation peak versus controlled axial shifts.

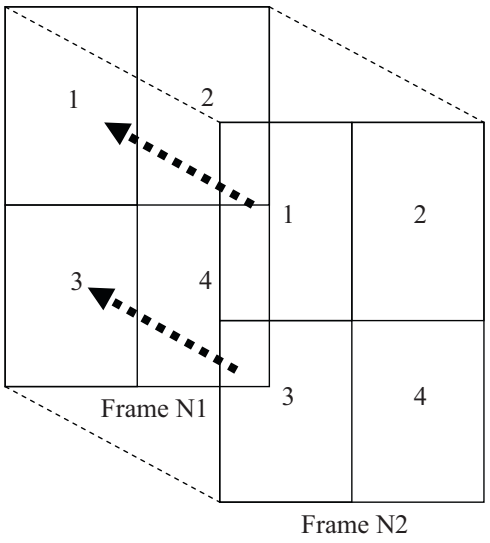

Fig. 9. Separate segments processing of the sub-divided images. Each segment is processed separately all over the time sequence.

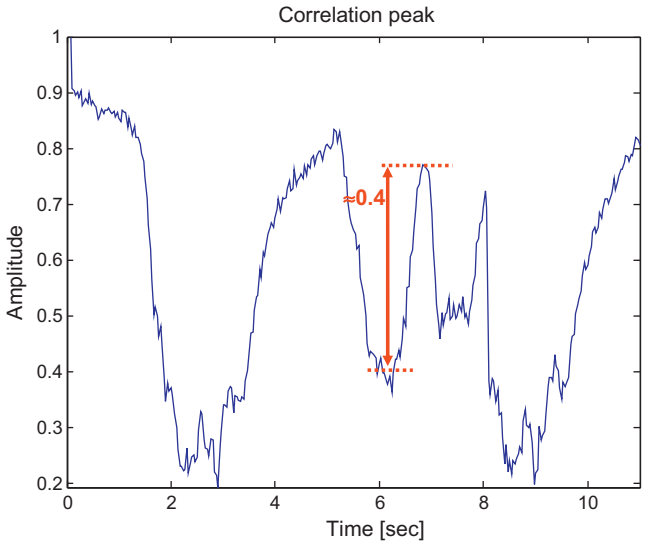

Fig. 8. Normalized correlation peak of first frame with other frames that is used for tracking of axial movement of rat's cardiac muscle cells.

was confined to approximately the cross-section of a single cardio-myocyte.

In the experiment we have used Olympus objectives of UPlanSApo 10×/0.40NA. Cells were illuminated with green laser DPSS type (Photop DPGL-2100) having a coherence length of several millimeters and beam diameter of 1.2 mm with divergence of 1.2 mrad. The wavelength was 532 nm and the illumination was performed from an oblique angle of about 30° with an output optical power of 30 mW and imaged through the objective lens of the microscope with proper defocusing as was stated before. A beam size as imaged on the cells was about 3 mm in diameter. Notice that, as explained before, we chose deliberately to have the illumination angle higher than the angle defined by the NA of the microscope lens (NA = 0.4 → θ = 23.5°, approximately). This was done to avoid collecting directly transmitted illumination.

The image was captured with Pixelink PL-A741-E camera having pixel size of 6.7 μm × 6.7 μm. The camera was connected to the microscope. The output of the camera was connected to a computer which was capturing video frames using the manufacturer software. The captured video was analyzed by MATLAB software.

The setup is very sensitive and also suitable for voice and heart beat detection. However, that was obtained when the measurement was done directly from the sound source itself. Secondary

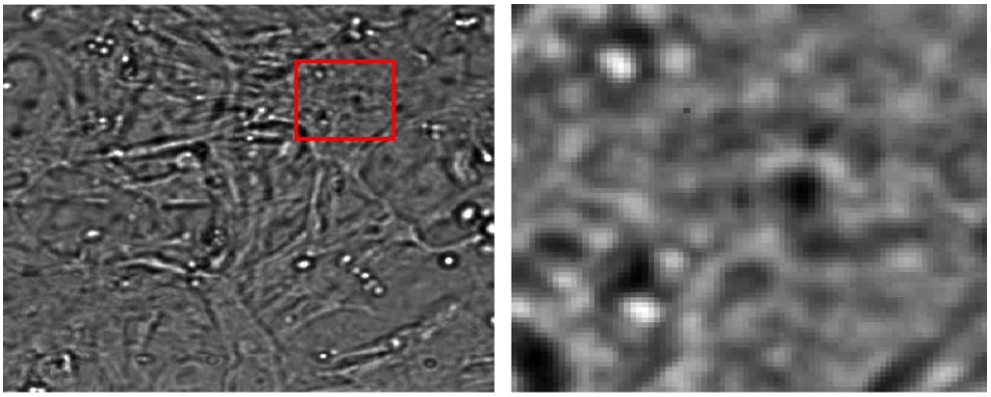

Fig. 10. (a). White illumination muscular cell image, with marked area of the internal part of the cell that had been chosen for fragmented processing. (b) Zoom over the inner marked area that was marked in (a).

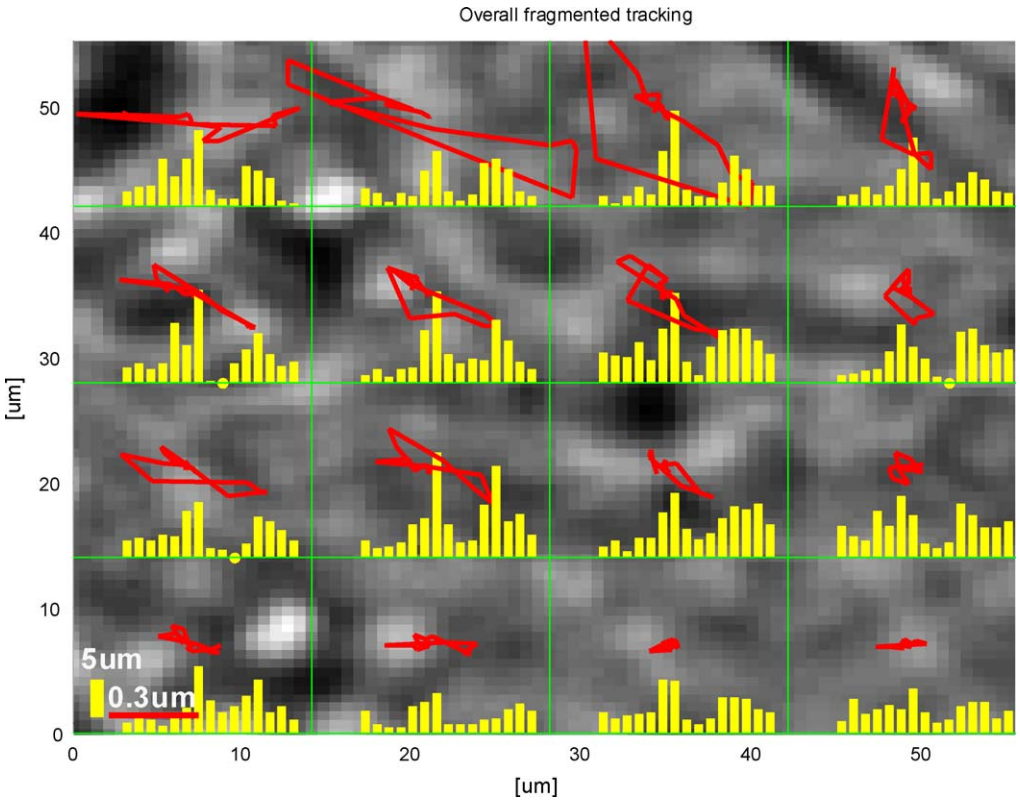

Fig. 11. Overall time-variant 3-D movement of fragmented cell areas. The red lines represent the *X*–*Y* movement, starting from origin (center of each area). The yellow bars represent the axial movement versus time (starting from left to right). In the left bottom corner we marked the scale for the lines and bars as 300 nm and 5 μm, respectively (For interpretation of references to colour in this figure legend, the reader is referred to the web version of this article.).

reflections of voice signals are too weak to affect our measurement. In addition during recording, quite conditions were imposed in the room. Various other vibration noises do not interfere with our measurement either. It is not difficult to perform the measurement in stable and non-noisy environment (the microscope was positioned on a vibration isolation table) exactly as it is possible to construct stable interference measurements. As was demonstrated in our calibration process in which a controlled movement was generated via the axially moving stage, we were easily able to obtain steady readout when no movement was generated. In addition it should also be noted that various noises can be filtered out since their vibration is random or has typical parameters while the movement of living cells is much less "artificial". The noises parameters/statistics can be extracted during the calibration process.

4. Experimental results

In Fig. 4 we present images from a sequence extracted from video recording using regular white light illumination. In Fig. 4(a) one may see the image captured just before contraction. In Fig. 4(b) we show the image of maximum contraction and in Fig. 4(c) the maximum expansion of the cell after contraction is presented. In the upper left corner of Fig. 4(a)–(c) we present a zoom image of the cell marked by the white rectangle in the non-zoomed image. In Fig. 4(d) we present the image of differences for the zoomed region appearing in the white rectangle of Fig. 4(a) and 4(b) in order to demonstrate that indeed contraction has occurred. Scale bar of 20 μm is provided at the left bottom of the Fig. 4(a).

The contraction presented in Fig. 4 was tracked using the speckle based approach that was previously described in Zalevsky and Garcia (2008) and Zalevsky et al. (2009). The obtained results can be seen in Fig. 5. The movement tracking presented in Fig. 5 is the 2-D projection of the 3-D movement of the cell (*X* and *Y* axes projection). In the figure one may see how these cells repeatedly expand and shrink in fixed intervals. The vertical units in Fig. 5 are displacement of the cells in micrometers (computed according to camera's pixels) and the horizontal axis is the temporal frames that are captured at rate of 30 fps. The analyzed region of interest was of 80 × 80 pixels. In the lower part of the image one may see a single diffused speckle pattern that was used to perform the movement tracking. Sometimes it is difficult to align the system on a specific spatial region of interest (ROI) of the cell using the laser illumination. In order to do a precise alignment, we first "lock" the system under white illumination, and then turn on the laser illumination (without white light) while preserving the same ROI.

If we observe again Fig. 5, one may see that movements of even less than 50 nm (in the vertical axis) were detected. The calculations of the obtained displacement (the vertical axis) was obtained using the following relations: the output of the algorithm is the displacement of the correlation peak (displacement of the cell picture between two sequential frames) measured in pixels. Since an objective of 10× was used, the equivalent cell movement imaged onto the detector plane was the size of a pixel divided by the magnification factor i.e. 6.7 μm/10 = 670 nm. If movement of 1/20 of a pixel in the detector plane is recognizable (as we have obtained in our experiments), then we obtain accuracy of approximately 35 nm. As mentioned before this accuracy of the optical configuration in tracking cell movement includes tracking this movement not only in the transverse plane but also movement due to their tilt and axial related shifts.

In Fig. 6 we present a reference test that was preformed over a culture with dead cells (no movement). This measurement is very important to demonstrate that indeed the measurements of Fig. 5 are not random, but rather correspond to real movement. As one may see from Fig. 6, there is almost a constant noise pattern that

corresponds to negligible values of displacement that are being obtained.

In Fig. 7 we present the experimental calibration which allows the measurement of the object's axial movement. The measurement was performed using the same configuration as in the previous experiment. We have positioned a reflective (non-transitive) object (placed instead of the cavity appearing in Fig. 3(b)) connected to a nanometer controlled stage (type: PI-515 with servo

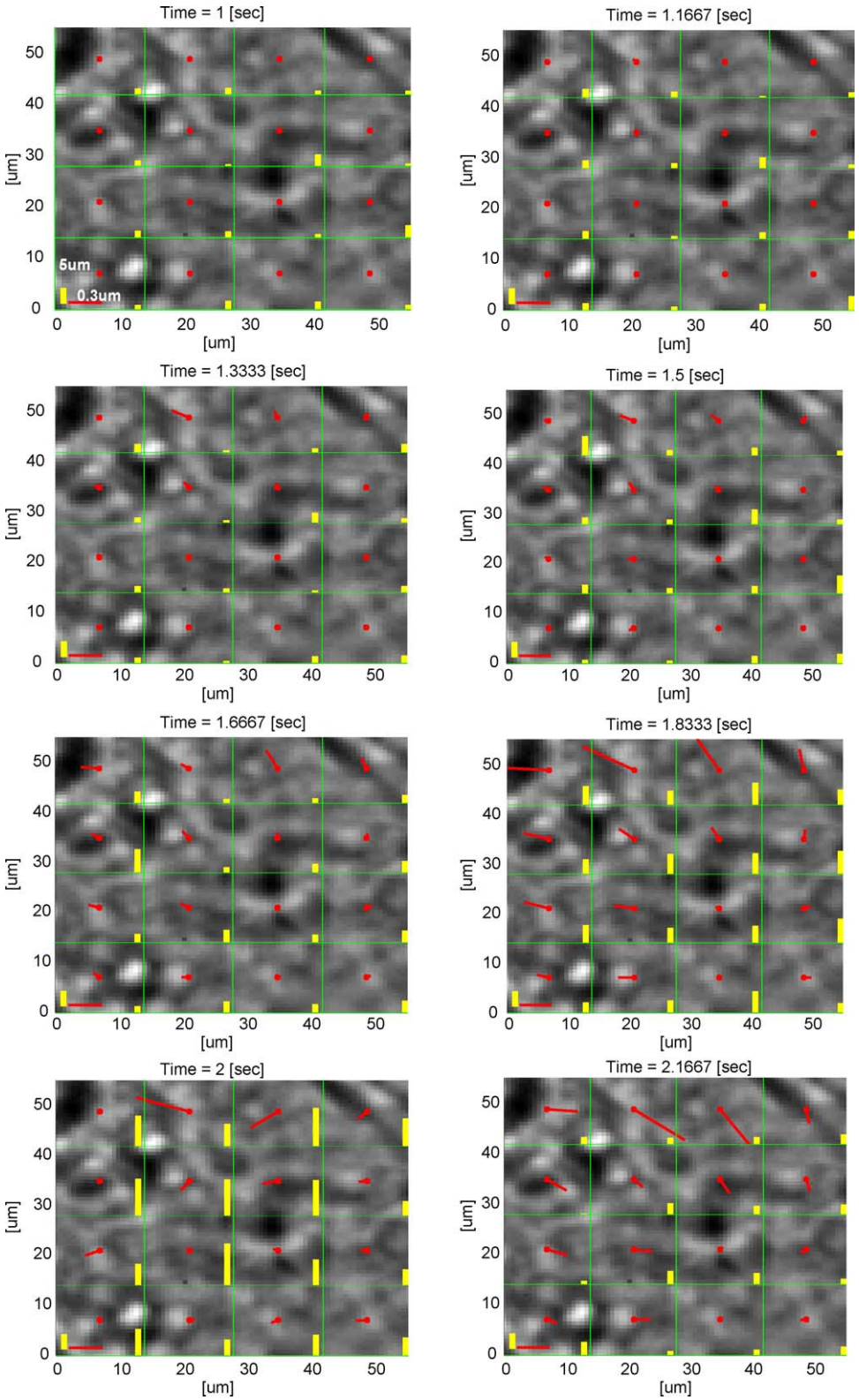

Fig. 12. Temporal evolving of the 3-D movement mapping of the cells. The dot represents the geometrical center of the processed ROI. The background is a picture of the cell taken with white light illumination. The red lines represent the relative *X*–*Y* movement (starting from the center of each area). The yellow bars represent the axial movement versus time (starting from left to right). In the left bottom corner we marked the scale for the lines and bars as 300 nm and 5 μm respectively (those numbers appear in the first image obtained for time = 1 s) (For interpretation of references to colour in this figure legend, the reader is referred to the web version of this article.).

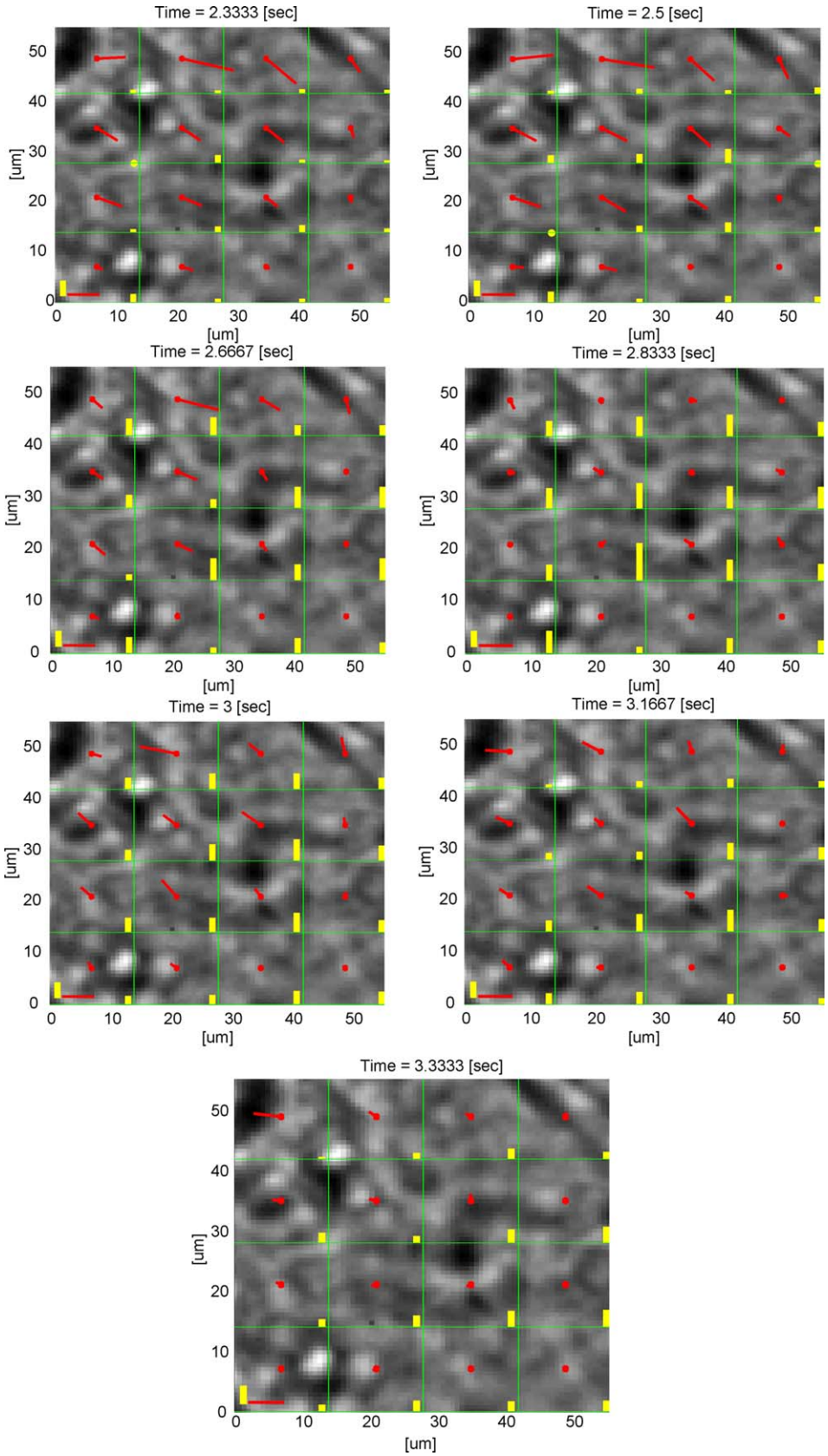

Fig. 12. (*Continued*.)

controller) that is capable of shifting the object in the axial dimension. We have illuminated the object with the same green laser. For each movement we have measured the obtained correlation peak while trying to show the relation existing between the value of this peak and the axial displacement.

To demonstrate repeatability, we repeated the experiment with different movement steps of 50 nm, 100 nm and 200 nm with the same stage. One may see that for all steps almost full coincidence occurs. If the signal to noise ratio allows detection of a 1% change in the height of the correlation peaks it means that the detection accuracy for the axial movement is about 200 nm.

In Fig. 8 we present how the *Z*-movement calibration chart of Fig. 7 was applied to track the *Z* movement of rat cardiac muscle cells. The figure shows the normalized correlation peak of the first frame with other frames. By comparing the change in the amplitude of the correlation peak one may see that for instance the 0.4 change in the value of the correlation peak corresponds to axial movement of approximately 6 μm (following the calibration presented in Fig. 7). Note that when we say movement (e.g., of 6 μm) we refer to the change in the optical path, i.e. the product between the change in the refractive index (obtained due to the contraction of the cell) and the actual displacement. In general, muscle cells normally contract at constant volume. Therefore, variations in length are compensated by thickening. Also the refractive indexes within a cell vary, for example, when actin and myosin overlap during movement.

The direction (up and down) of the axial displacement cannot be calculated as straightforwardly, because the same movement in both directions causes the same change in the peak value. However, using a priori knowledge about the nature of the movement of the object, one may choose the right frame rate (according to Nyquist sampling law it should be two times faster than the fastest movement) and later on track the axial movement sequence (extracted by the algorithm) in such a way that every zero-crossing point (point of focus) designates a change in the movement direction.

5. Measuring 3-D map and flow distribution

In Figs. 5 and 8 we measured the movement of the entire cardiac muscle cell (or of its center of mass). Now the challenge is to map the 3-D movement inside a given cell while doing the tracking individually over 4 by 4 segments inside a given cell. Thus, we are not trying to track the center of the optical density. Conversely, we are trying to show that the cell is not rigid and thus it is not moving as one unit. Rather, the cell has different movement parameters in each of its different segments.

In doing this experiment we used the same constructed module to map the movement of spatial segments within the cell. The experiment was preformed exactly as the previous ones. The difference was only at the processing part. The extracted results were obtained by spatially dividing each image in the sequence into 4 by 4 resolution regions. Each region was considered as a separate disconnected segment and was processed separately over the entire time sequence. Schematic representation of the fragmentation of the sequence is given at Fig. 9. Separate processing of each segment images is shown. Each segment is processed separately all over the time sequence, thus segment #1 in frame N1 was correlated with segment #1 in frame N2 etc. Therefore, in each region the correlation was computed between two adjacent images in the sequence. From the position of the correlation peak we estimated the in-plane 2-D movement of the cells and from the value of the correlation peak we extracted the axial movement of the relevant segment. The conversion of the correlation peak value to axial displacement was done following the calibration presented in Fig. 7. Since the processing was applied in each of the 4 by 4 resolution regions, a 3-D displacement map of the cell was extracted.

Fig. 10(a) presents the white illumination muscular cell image, with the marked area of internal part of the cell that had been chosen for fragmented processing. Fig. 10(b) is a zoom over the inner marked area that was marked in Fig. 10(a).

The obtained experimental results for the 3-D mapping can be seen in Figs. 11 and 12. In Fig. 11 we present the overall time-variant 3-D movement of fragmented cell areas. The red lines represent the *X*–*Y* movement, starting from the origin (center of each area). The yellow bars represent the axial movement versus time (starting from left to right). In the left bottom corner we marked the scale for the lines and bars as 300 nm and 5 μm, respectively. Note once again that what we track is not the movement, but rather the temporal change of the *optical path*. Therefore, physical movement as well as variation of the refraction index will cause similar effects in our measurement.

In Fig. 12 we present the temporal evolution of the 3-D movement mapping of the cells. A dot represents a geometrical center of the processed ROI. The background of the figure is a picture of the cell taken in white illumination (constant all over the sequence). The red lines represent the relative *X*–*Y* movement between two adjustment frames shown in the figure and the geometrical center of each segment marks the origin of the relative vector of movement. The yellow bars represent the axial movement versus time (starting from left to right). In the left bottom corner we marked the scale for the lines and bars as 300 nm and 5 μm respectively (those numbers appear in the first image obtained for Time = 1 s). The sampling time of each movement map is designated on top of the image. The time difference between images is of about 0.166 s.

Note that the background on top of which we present the movement of the different segments in the cell is a static internal region of the cell. It looks noisy since the magnification was only ×10. However please note that the image of the cell itself is irrelevant to the accuracy of the 3-D movement information that we extract. For the 3-D movement we do not use the image of the cell, (obtained with white light illumination) rather we use the speckle pattern obtained with green laser illumination whose signal to noise ratio is very high. In practice, the signal to noise ratio of the output of our algorithm that extracts the 3-D movement was very high, above 10 dB, which gave us confidence in the reliability of the experimentally obtained results.

6. Conclusions

In this paper we have presented a transmissive speckle based configuration to track movement of rat cardiac muscle cells. Unlike transmission interferometry based approaches, the discussed technique can accurately track not only transverse and tilt movement but also axial shift and thus is suitable for biological applications where 3-D movement exists. Experimental mapping of general 3-D movement as well as the movement of spatial segments inside rat cardiac muscle cells was demonstrated.

The basic modification of the speckle based interferometric configuration is related to the slight image defocusing provided by the imaging lens. This defocusing allowed the conversion of the modification of the speckle patterns due to tilting movement (as occurs in regular speckle based interferometry) into shifts of the same unchanged pattern.

References

Burlew, B.S., Weber, K.T., 2000. Connective tissue and the heart. Functional significance and regulatory mechanisms. Cardiol. Clin. 18, 435–442.

Calaghan, S.C., White, E., 1999. The role of calcium in the response of cardiac muscle to stretch. Prog. Biophys. Mol. Biol. 71, 59–90.
Dubois, F., Callens, N., Yourassowsky, C., Hoyos, M., Kurowski, P., Monnom, O., 2006. Digital holographic microscopy with reduced spatial coherence for three-dimensional particle flow analysis. Appl. Opt. 45 (5), 864–871.
Fixler, D., Tirosh, R., Zinman, T., Shainberg, A., Deutsch, M., 2002. Differential aspects in ratio measurements of $[Ca^{2+}]i$ relaxation in cardiomyocyte contraction following various drug treatments. Cell Calcium 31, 279–287.
Fixler, D., Tirosh, R., Zinman, T., Sheinberg, A., Deutsch, M., 2003. Fluorescence polarization – a novel indicator of cardiomyocyte contraction. BBRC 300, 23–28.
Ikeda, T., Popescu, G., Dasari, R.R., Feld, M.S., 2005. Hilbert phase microscopy for investigating fast dynamics in transparent systems. Opt. Lett. 30, 1165–1167.
Leedertz, J.A., 1970. Interferometric displacement measurements on scattering surfaces utilizing speckle effects. J. Phys. E Sci. Instrum. 3, 214–218.
Leushacke, L., Kirchner, M., 1990. Three dimensional correlation coefficient of speckle intensity for rectangular and circular apertures. J. Opt. Soc. Am. A 7, 827–833.
Marquet, P., Rappaz, B., Magistretti, P.J., Cuche, E., Emery, Y., Colomb, T., Depeursinge, C., 2005. Digital holographic microscopy: a noninvasive contrast imaging technique allowing quantitative visualization of living cells with subwavelength axial accuracy. Opt. Lett. 30, 468–470.
Park, Y., Popescu, G., Badizadegan, K., Dasari, R.R., Feld, M.S., 2007. Fresnel particle tracing in three dimensions using diffraction phase microscopy. Opt. Lett. 32 (7).
Schnars, U., Jüptner, W., 1994. Direct recording of holograms by a CCD target and numerical reconstruction. Appl. Opt. 33, 179–181.
Shaked, N.T., Rinehart, M.T., Wax, A., 2009a. Dual-interference-channel quantitative-phase microscopy of live cell dynamics. Opt. Lett. 34, 767–769.
Shaked, N.T., Rinehart, M.T., Wax, A., 2009b. Dynamic quantitative phase microscopy of biological cells. In: Conference on Lasers and Electro-Optics/International Quantum Electronics Conference, OSA Technical Digest (CD), Optical Society of America, Paper CFA4.
Shaked, N.T., Zhu, Y., Rinehart, M.T., Wax, A., 2009c. Two-step-only phase-shifting interferometry with optimized detector bandwidth for microscopy of live cells. Opt. Exp. 17, 15585–15591.
Spurgeon, H.A., Steren, M.D., Baartz, G., et al., 1990. Simultaneous measurement of Ca^{++}, contraction, and potential in cardiac myocytes. Am. J. Physiol. 258, H574–H586.
Yamaguchi, I., Zhang, T., 1997. Phase-shifting digital holography. Opt. Lett. 22, 1268–1270.
Zalevsky, Z., Garcia, J., 2008. Motion detection system and method. Israeli Patent Application No. 184868 (July 2007). WO/2009/013738 International Application No. PCT/IL2008/001008 (July 2008).
Zalevsky, Z., Beiderman, Y., Margalit, I., Gingold, S., Teicher, M., Mico, V., Garcia, J., 2009. Simultaneous remote extraction of multiple speech sources and heart beats from secondary speckles pattern. Opt. Exp. 17, 21566–21580.